Canadian Journal of Fisheries and Aquatic Sciences

OPEN ACCESS | Research Article

Species distribution models estimate time-varying juvenile salmon distributions in the north- and southeastern Bering Sea

Lilian K.G. Hart[a], **Curry J. Cunningham**[a], **Ellen M. Yasumiishi**[b], **Franz J. Mueter**[a], **James T. Thorson**[c], **Jodi L. Pirtle**[d], **and J. Andrew Dimond**[b]

[a]College of Fisheries and Ocean Sciences, University of Alaska Fairbanks, 17101 Point Lena Loop Rd., Juneau, AK 99801, USA; [b]NOAA/NMFS, Auke Bay Laboratories Division, Alaska Fisheries Science Center, Ted Stevens Marine Research Institute, 17109 Point Lena Loop Road, Juneau, AK 99801, USA; [c]NOAA/NMFS, Resource Ecology and Fisheries Management Division, Alaska Fisheries Science Center, 7600 Sand Point Way NE, Seattle, WA 98115, USA; [d]NOAA/NMFS, Habitat Conservation Division, Alaska Region, Juneau Federal Building, P.O. Box 21668, Juneau, AK 99802-1668, USA

Corresponding author: **Lilian K.G. Hart** (email: lkhart2@alaska.edu)

Abstract

This study compares alternative implementations of species distribution models (SDMs) for quantifying static and dynamic patterns in marine habitat use, with a case study focusing on juvenile salmon in the eastern Bering Sea. We compare the performance of two prevalent SDM frameworks—generalized additive models (GAMs) and vector autoregressive spatio-temporal (VAST) models—in predicting juvenile salmon distributions and assessing interannual variation in habitat utilization. The two SDM frameworks produced similar spatial predictions but performed differently in tests of within-sample and out-of-sample predictive power. Our findings indicate that VAST models may provide more precise estimates of distribution compared to GAMs. Maps of predicted juvenile salmon distributions showed highest salmon densities in habitats within the 50 m isobath of the continental shelf, underscoring the importance of these coastal areas, although among-species differences were evident. Model performance results suggested evidence for spatial variation in juvenile salmon species' distributions through time. Our findings suggest that an SDM approach can be effective for estimating static and dynamic juvenile salmon distributions, and for providing insights that are useful in spatial fisheries management contexts.

Key words: salmon ecology, GAM, VAST, juvenile salmon, species distribution modeling, essential fish habitat

Introduction

Development and implementation of spatial management strategies in fisheries require comprehensive understanding of species' distribution in space, and the extent to which distributions change across time. In the United States, the Magnuson–Stevens Fishery Conservation and Management Act utilizes essential fish habitat (EFH) to ensure the conservation of "those waters and substrate necessary to (federally managed) fish for spawning, breeding, feeding, or growth to maturity" (16 U.S. Code § 1802). Knowledge of EFH informs conservation decisions and initiates cross-agency communication on fishing and/or nonfishing activities that may adversely affect EFH. Ecosystem approaches like the EFH regulations are implemented internationally, particularly in North America, Europe, and Australia (FAO 1995; Environment Protection and Biodiversity Conservation Act 1999; Malta MedFish4Ever Ministerial Declaration 2017; EU Action Plan 2023). Expanding habitat conservation planning to the ecosystem scale is an ongoing challenge, particularly for migratory species like salmon. EFH and other related ecosystem approaches have typically produced static representations of fish habitat, but these may fall short in the face of interannual variation in habitat utilization or climate-driven changes in species distribution.

Definition of EFH requires synthesis of available information on species' occurrence or habitat-related abundance across space. Species distribution models (SDMs) represent a contemporary, quantitative approach for describing spatial or spatio-temporal variations in habitat use and relationships with environmental covariates. As such, SDMs present an opportunity to standardize observations of presence and abundance of species based on fishery-independent survey data or fishery-dependent catch rates to describe both static and dynamic EFH. Spatio-temporal SDMs have been widely utilized in fisheries research to standardize indices of abundance (Thorson and Barnett 2017; Grüss et al. 2019; Maunder et al. 2020) for stock assessment, and measure the impacts of past climate variability on species distributions (Mueter and Litzow 2008; Thorson 2019*a*; Yasumiishi et al. 2020; Brodie et al. 2021). However, in the context of updating EFH

definitions, spatio-temporal SDMs are a relatively novel approach (Laman et al. 2018; Harris et al. 2023; Pirtle et al. 2024).

There exists a diversity of statistical frameworks for constructing spatio-temporal SDMs. Two commonly applied spatio-temporal SDM frameworks within fisheries are generalized additive models (GAMs) and vector autoregressive spatio-temporal (VAST) models. A GAM is a generalized linear model with a linear predictor that captures nonlinear variability as a sum of smooth functions of the predictor variables (Wood 2006). GAMs describe flexible, nonparametric relationships between predictors and the response variable, and can represent both spatial and spatio-temporal variation as the smoothed interaction between latitude, longitude, and possibly time. VAST models are a class of spatio-temporal SDMs that integrate autoregressive time components and spatial random effects (Thorson and Barnett 2017). VAST models, unlike GAMs, explicitly model spatial and/or temporal correlation among observations, and are specifically designed for modeling multivariate time series data. Another notable difference between the two SDM frameworks lies in their approaches to prediction; GAMs provide predictions for specific input values, whereas VAST generates a network of polygons across the spatial domain for which abundance and occurrence may be predicted. GAMs have wide application in research related to spatial ecology, and were used to refine EFH definitions for Alaska groundfish and crab species in the 2018 EFH review (Laman et al. 2018) and as ensemble SDM (e-SDM) constituents for the 2023 EFH review (Harris et al. 2022, 2023; Laman et al. 2022; Pirtle et al. 2023, 2024). VAST models have been employed within stock, habitat, climate, and ecosystem assessments (see Thorson (2019*b*) for a list of early studies), and are actively being developed for a variety of quantitative fisheries science applications, including extending SDMs to estimate spatially varying coefficients (Thorson et al. 2023), account for spatially varying catchability (Grüss et al. 2023), and for building stream networks to relate changes in freshwater fish distributions to fish length and river habitat attributes (Charsley et al. 2023).

Despite the applicability of these two statistical frameworks in quantifying spatial and spatio-temporal variation in fish abundance and occurrence, there remains an opportunity to evaluate tradeoffs among these methods in describing EFH. There has been limited research directly comparing their performance in describing species distributions (but see Brodie et al. 2020). Brodie et al. (2020) found that VAST models estimated abundance trends more precisely than GAMs when fit to empirical data for three species (arrowtooth flounder *Atheresthes stomias*, Pacific cod *Gadus macrocephalus*, and walleye pollock *Gadus chalcogrammus*). However, the performance of candidate SDM frameworks are likely context dependent, influenced by both the spatial dynamics of the focal species and aspects of the observation or sampling process. At the same time, there exists a need to identify applicable SDM methods for refining EFH descriptions for juvenile salmonids in their ocean life history stages, including in the eastern Bering Sea (EBS) region of Alaska.

Current EFH maps for juvenile salmon in the marine waters surrounding Alaska were created using empirical cumulative distribution function (ECDF) methods that associated salmon occurrence with habitat conditions, including sea surface temperature, sea surface salinity, and bottom depth (Echave et al. 2012). The extent of juvenile salmon ocean life history stage EFH, as defined by the ECDF methods, extends along the entire continental shelf and slope between the Chukchi Sea and the Dixon Entrance in the area of the U.S. Exclusive Economic Zone off Alaska (NPFMC 2024). The mapping methods employed in 2012 represented the best-available-science at the time, but the authors of the study recognized the risk of such broad EFH descriptions. Broad EFH descriptions dilute the effective power of EFH and the utility of EFH maps by reducing the credibility and actionability of the data at the scales demanded by management organizations and processes (Echave et al. 2012).

Our study compared the use of GAMs and VAST for describing the distributions of juvenile salmon species in the EBS, and reflected on the application of SDM results to update juvenile salmon EFH definitions in this region. The first objective of this study was to compare the performance of the two applicable SDM frameworks represented by GAMs and VAST models, based on within and out-of-sample performance metrics. The second objective was to describe the species-specific average distribution of juvenile salmon in the EBS using SDMs, with a view toward updating existing EFH definitions for this life stage. Five species of Pacific salmon that are endemic to the EBS were considered in this analysis: Chinook salmon (*Oncorhynchus tshawytscha*), chum salmon (*Oncorhynchus keta*), coho salmon (*Oncorhynchus kisutch*), pink salmon (*Oncorhynchus gorbuscha*), and sockeye salmon (*Oncorhynchus nerka*). The third objective of this study was to quantify the temporal variation in the core distribution areas occupied by juvenile salmon in the EBS; specifically, to assess whether core areas persist or shift through time. Prior research into connections between salmon marine distribution and climate, including juvenile salmon in the EBS (Yasumiishi et al. 2020) and Chinook salmon along the West Coast of the United States (Shelton et al. 2021) found evidence for nonlinear and possibly stock-specific changes to distributions and abundance in response to climate warming.

Methods

To describe spatial and spatio-temporal variation in juvenile salmonid abundance-density, four SDM variants of increasing complexity were implemented as parallel model structures within the GAM and VAST frameworks, totaling eight candidate SDMs (Table 1). These four model variants, with approximately parallel implementations in GAM and VAST frameworks, build layers of complexity upon the null model (Model StaticN) by (1) adding interannual variation in total catch across space (Model StaticYr), (2) spatio-temporal variation with temporal autocorrelation (Model SpatiotA), and (3) spatio-temporal variation that was independent among years (Model SpatiotB). The functional form of the most complex model variant is described below (eq. 1; Model SpatiotB), with all other variants (i.e., models StaticN, StaticYr, and SpatiotA) representing simplified versions

of this most flexible form (Table 1).

$$\ln\left(A\left(s_i,\ t_i\right)\right) = \beta_0 + f_1\left(s_i\right) + \beta_{t_i} + f_{t_i}\left(s_i\right) + o\left(\ln\left(k_i\right)\right) \quad (1)$$

Equation 1 describes the predicted natural log of catch in numbers for a given location in space s_i and year of sampling t_i for observation i, where space is represented by latitude and longitude coordinates. Predicted abundance (A) is an additive function of average abundance across space and time β_0, an average spatial field $f_1\left(s_i\right)$ (spatial effects), categorical (factor) year effects β_{ti} (temporal effects), and year-specific spatio-temporal fields $f_{t_i}\left(s_i\right)$ (spatio-temporal effects), with an offset (o) for the natural log of effort k in area swept (km^2). Vessel effects were tested during exploratory data analysis with one species (Chinook). Overall vessel effects had a small effect size that was not statistically distinguishable from zero at the $p = 0.05$ level in explaining variation in catch observations, and were therefore not included in subsequent analyses.

This study paid particular attention to the configuration of spatio-temporal GAMs in the implementation of smooth functions. Thin plate splines were specified for the tensor product spatial smooths in all GAM variants to accommodate expected anisotropy in the response to latitude and longitude. The Model SpatiotA variants, which contained smoothed three-way space–time interaction terms $f_2\left(s_i, t_i\right)$, used a thin plate basis for the spatial component, and a cubic spline basis for the temporal component. To address unreasonably high predictions of abundance in areas with few observations, we limited model predictions to values within the range of encounter data by setting the smoothing penalty to affect the first derivative (Barnes et al. 2022; Harris et al. 2023). To effectively handle catch data with many zeros, we specified a Tweedie distribution within the GAM framework for the error structure, with a log link function (Shono 2008).

VAST models were configured to approximate the four GAM structures described previously (Table 1). To the extent possible, parallel model structures were implemented to allow comparison of model performance among GAM and VAST models of increasing complexity. Zero-inflation was accounted for within VAST models by specifying a Poisson-link delta model, which approximates the Tweedie distribution in a computationally efficient manner. The gamma distribution was selected to model the positive catch component, following recommendations from a case study (Thorson 2021). Estimation of VAST spatio-temporal fields was turned off for the static models (Models StaticN–StaticT), while spatio-temporal fields were estimated for the time-varying spatio-temporal models (Models SpatiotA–SpatiotB). A constant-intercept-only VAST null model was also fit for each model variant to calculate percent deviance explained relative to this alternative. The equation used to calculate percent deviance explained of VAST model variants is described below (eq. 2), where D_{M_i} represents the deviance of the model of interest, and D_{M_n} represents the deviance of the VAST null model.

$$\%\ \text{Deviance Explained} = \frac{1 - D_{M_i}}{D_{M_n}} \quad (2)$$

Table 1. Species distribution model descriptions and their implementation in mgcv.

Model name	Description	Equation	mgcv Implementation
Model StaticN	Static (null) model representing long-term average spatial variation	$\ln\left(A\left(s_i,\ t_i\right)\right) = \beta_0 + f_1\left(s_i\right) + o\left(\ln\left(k_i\right)\right)$	gam(Catch) ~ te(Lon, Lat, bs = "tp," k = 9, m = 1) + offset(log(Effort))
Model StaticT	Static model with interannual variability in abundance	$\ln\left(A\left(s_i, t_i\right)\right) = \beta_0 + f_1\left(s_i\right) + \beta_{t_i} + o\left(\ln\left(k_i\right)\right)$	gam(Catch) ~ te(Lon, Lat, bs = "tp," k = 9, m = 1) + offset(log(Effort)) + fac(Year)
Model SpatiotA	Dynamic model capturing spatio-temporal autocorrelation	$\ln\left(A\left(s_i, t_i\right)\right) = \beta_0 + f_1\left(s_i\right) + \beta_{t_i} + f_2\left(s_i, t_i\right) + o\left(\ln\left(k_i\right)\right)$	gam(Catch ~ te(Lon, Lat, bs = "tp," k = 9, m = 1) + offset(log(Effort)) fac(Year) + te(Lon, Lat, Year, d = c(2,1), bs = c("tp," "cr"), k = 9, m = 1)
Model SpatiotB	Dynamic model with independent yearly spatial fields	$\ln\left(A\left(s_i,\ t_i\right)\right) = \beta_0 + f_1\left(s_i\right) + \beta_{t_i} + f_{t_i}\left(s_i\right) + o\left(\ln\left(k_i\right)\right)$	gam(Catch ~ te(Lon, Lat, bs = "tp," k = 9) + offset(log(Effort)) + fac(Year) + te(Lon, Lat, by = fac(Year), bs = "tp," k = 9)

Note: Abundance at location s and time t is modeled as a log response to the additive functions of a long-term average spatial pattern $f_1\left(s_i\right)$, average abundance across space and time β_{t_i}, plus any additional parameters to account for interannual variability and shifts in distribution.

The eight candidate SDM structures were applied to estimate juvenile salmon distributions in the EBS. The Bering Sea represents important habitat for Pacific salmon while they forage and grow at sea. Major freshwater systems connected to the EBS that have historically supported abundant salmon runs include the rivers of Bristol Bay, the Yukon River, and the Kuskokwim River. The southern EBS shelf represents an important ocean migration corridor for Bristol Bay juvenile sockeye salmon (Farley et al. 2005), and EBS juvenile pink salmon likely also utilize the continental shelf as a migration corridor as they head south toward overwintering habitat in the north Pacific Ocean (Beamish 2018). Distribution models of high-seas salmon data have highlighted high predicted relative abundance of Chinook salmon along the EBS shelf during the summer months (Langan et al. 2024). Additionally, life history models identified juvenile salmon abundance in the northern Bering Sea as significantly related to the number of adult salmon returning to natal freshwaters (Farley et al. 2020).

Surface trawl survey data from the Bering–Arctic–Subarctic Integrated Survey (BASIS) were used to inform models for each species of Pacific salmon endemic to the EBS. BASIS was initiated in 2002 by the National Marine Fisheries Service to improve the understanding of salmon life histories and ecology in the Bering Sea (Murphy et al. 2021). Time series of spatially referenced catch and effort data from BASIS are publicly available through the Alaska Ocean Observing System portal. The survey consists of surface trawls conducted annually between the months of August and October. The sampling design, roughly centered around the coastal domain of the northern EBS shelf (Murphy et al. 2017), has varied considerably among years due to survey objectives and available sampling effort (Fig. 1). The area of the Bering Sea within ~55°–65°N and ~160°–173°W has received the most consistent survey sampling, while the Chukchi Sea has been sampled intermittently. The number of stations comprising the survey each year ranged from 31 stations in 2008 to 159 stations in 2010, with a median value of 125 stations. Fish caught in the trawl are identified to species and then subsamples are weighed, counted, and further processed according to species protocols (McKelvey and Williams 2018). Sampling effort in units of area swept (km^2) is associated with each survey tow, calculated based on the horizontal opening from the net sonar and the distance from GPS (global positioning system) locations at the start and end of the trawl set (Murphy et al. 2021).

Data were filtered to remove sampling events where problems with gear or unsatisfactory tows occurred. Initial exploration revealed large differences in the number of positive catch records for each species of salmon. Chum and pink salmon were encountered most frequently across years (53% and 50%, respectively), followed by Chinook salmon (37%), sockeye salmon (37%), and coho salmon (31%). Due to low catch rates for coho salmon and model convergence issues, we did not consider this species in further analysis. While the BASIS sample design occasionally included the Chukchi Sea and areas south of the Aleutian Islands, data were clipped to a region of interest encompassing the north eastern Bering Sea (NEBS) and southeastern Bering Sea (SEBS) (Supplementary Fig. S9) to eliminate areas with consistently low sampling effort.

Following inspection of model diagnostic plots (quantile–quantile plots, residual maps) (Supplementary Figs. S1–S8), models that converged were then used to predict salmon abundance across the area of interest (AOI) (Supplementary Fig. S9) (i.e., extrapolation grid) in the NEBS and SEBS. We defined the spatial extent of the extrapolation grid manually by selecting points around survey stations in the AOI, converting these coordinates to a spatial polygon, generating a regional grid (resolution = 0.002 km^2), and clipping the grid to the extent of the spatial polygon (knots = 162 174) (R packages "rgdal", "sf", and "sp"; Pebesma and Bivand 2005; Bivand et al. 2013; Pebesma 2018; Bivand et al. 2023). This clipped grid was also used to derive prediction surfaces for the GAM predictions of abundance density. To overcome computational demands resulting from the large number of spatial prediction locations in the VAST grid, n = 10 000 latitude and longitude locations from this grid were randomly sampled without replacement and saved as a new grid file. Predictions from GAMs were generated using the predict() function from the "mgcv" package (Wood et al. 2016). Both VAST and GAM predictions were then mapped with the "ggplot2" (Wickham 2016), "rnaturalearth" (Massicotte and South 2023), and "akgfmaps" (Rohan 2023) packages.

The performance of the two SDM frameworks, GAMs and VAST, were compared quantitatively using percent deviance explained for within-sample predictive performance, and 10-fold cross-validation to assess out-of-sample predictive performance (Thorson and Barnett 2017). For cross-validation, the data were partitioned by randomly assigning each survey haul record a fold value from 1 to 10 (total 1845 records per species). These fold values were then used to subset the original dataset into testing and training subsets, for a total of 10 sets of testing and training data. Following partitioning, each of the candidate statistical models were fit to the training data. These models were subsequently used to predict the expected value of the response variable (abundance) for the testing data. Negative log likelihood (NLL) scores for GAMs were calculated following a three-step approach. First, Tweedie dispersion and power term values were extracted from the GAM model object. These dispersion and power term values were then used to calculate the likelihood of the observations in the testing dataset. Finally, the likelihood was log-transformed and multiplied by negative one to form the NLL value. The NLL of the model was summed across the 10-folds to create a total out-of-sample NLL for a given model, describing out of sample predictive performance for a fitted model. A lower NLL indicates higher out-of-sample predictive power. Information theory (Akaike information criterion; Burnham and Anderson 2002) and percent deviance explained were used to compare model performance and to evaluate whether there was model-based statistical evidence for shifts in species distributions through time.

Model residuals were calculated according to the SDM framework. Quantile residuals were calculated for GAMs, while DHARMa residuals were calculated for VAST models. Both residual types are scaled, but DHARMa residuals are the

Fig. 1. Maps showing the sampling design of the Bering–Arctic–Subarctic Integrated Survey from 2002 to 2019, with survey stations represented as black points over gray marine waters bordered by polygons of the land masses of Russia's Chukchi Peninsula, and Alaska. Basemap: *rnaturalearth* (Massicotte and South 2023), Projection: Alaska Albers Conic Equal Area, Datum: NAD83, EPSG code: 3338, Coordinates = Cartesian 2D.

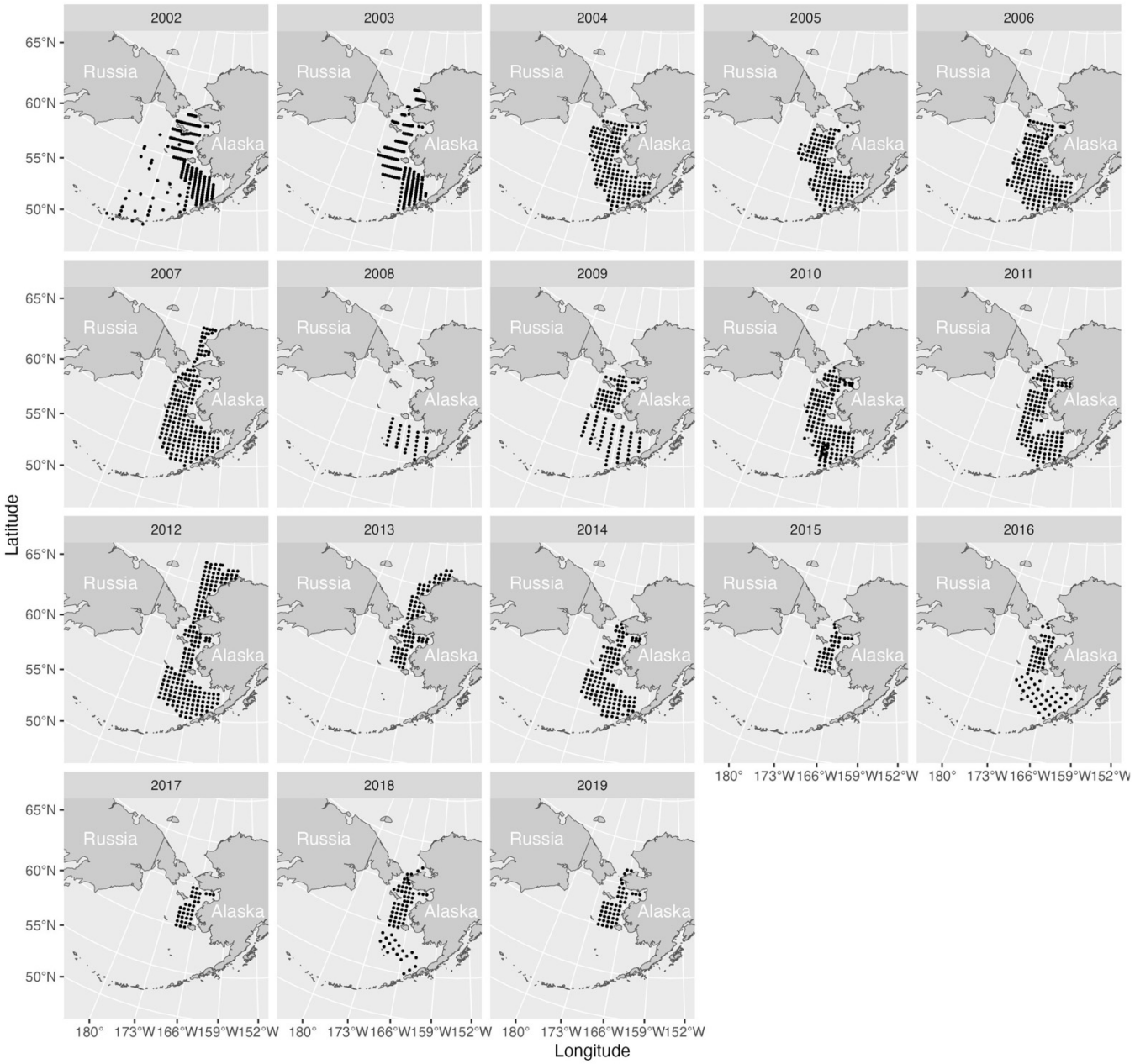

preferred method for mixed effects models and were therefore more suitable for the VAST framework. Quantile residuals were calculated in R from saved GAM model objects using the "statmod" package (Dunn and Smyth 1996). Scaled quantile residuals ("DHARMa residuals") were extracted from standard VAST reports associated with each fitted VAST model.

Maps of predicted juvenile salmon distributions conditional on SDMs were generated to compare model-predicted habitat areas against those described empirically in the literature, and to assess the application of SDMs to juvenile salmon EFH descriptions. The latest Alaska EFH 5-year review produced EFH maps by representing the area circumscribing the top 95% of SDM-predicted abundance (Pirtle et al. 2024). In this study, individual static and spatio-temporal model predictions of juvenile salmon distributions were used to create static and dynamic EFH and Core EFH maps. For each species and model type, we calculated the cumulative sum of abundance predictions and retained those comprising the top 95% (EFH) and 50% (Core EFH) of predicted abundance. The areas encompassed by static SDM-based EFH definitions were calculated and compared against those areas delineated by current official EFH definitions (NPFMC 2024). Prediction points were aggregated and converted to spatial polygons (R package "concaveman"; Gombin et al. 2020). The areas of these spatial

Table 2. Model performance metrics used for within-framework model evaluation (AIC, % deviance explained (DE)) and for cross-framework evaluation (% deviance explained (DE), negative log likelihood (NLL)).

Species	Model structure	AIC (GAM)	AIC (VAST)	% DE (GAM)	% DE (VAST)	NLL (GAM)	NLL (VAST)
Chinook	Model StaticN: (Static) Average spatial field	5295	5261	53%	38%	2704	2633
	Model StaticT: (Static) Average spatial field with factor year effect	5187	5094	58%	44%	2653	2552
	Model SpatiotA: (Dynamic) Model capturing spatio-temporal autocorrelation	5029	5049	65%	52%	2604	2551
	Model SpatiotB: (Dynamic) Spatio-temporal model with independent spatial fields	NA	5015	NA	64%	NA	2769
Chum	Model StaticN: (Static) Average spatial field	10 621	10 555	32%	26%	5420	5419
	Model StaticT: (Static) Average spatial field with factor year effect	10 475	10 145	39%	36%	5362	5198
	Model SpatiotA: (Dynamic) Model capturing spatio-temporal autocorrelation	10 237	9942	49%	54%	5303	5195
	Model SpatiotB: (Dynamic) Spatio-temporal model with independent spatial fields	9628	9774	80%	71%	6747	5997
Pink	Model StaticN: (Static) Average spatial field	10 097	10 054	26%	22%	5160	5138
	Model StaticT: (Static) Average spatial field with factor year effect	9753	9557	42%	38%	5136	5040
	Model SpatiotA: (Dynamic) Model capturing spatio-temporal autocorrelation	9524	9401	53%	55%	5215	5106
	Model SpatiotB: (Dynamic) Spatio-temporal model with independent spatial fields	9054	9209	79%	69%	6625	5586
Sockeye	Model StaticN: (Static) Average spatial field	8700	8677	43%	32%	4441	4421
	Model StaticT: (Static) Average spatial field with factor year effect	8419	8228	55%	43%	4316	4216
	Model SpatiotA: (Dynamic) Model capturing spatio-temporal autocorrelation	8104	8101	68%	59%	4203	4208
	Model SpatiotB: (Dynamic) Spatio-temporal model with independent spatial fields	7928	8002	81%	70%	5477	4553

Note: GAM, generalized additive model; VAST, vector autoregressive spatio-temporal.

Table 3. Calculated areas of model-predicted essential fish habitat (EFH) in square kilometers, and their size relative to the current official Alaska juvenile salmon EFH definitions from National Oceanic and Atmospheric Administration (NOAA) National Marine Fisheries Service (NMFS) Alaska Fisheries Science Center (AFSC) Technical Memorandum NMFS-AFSC-236.

Species	GAM-predicted EFH area	VAST-predicted EFH area	Official EFH area clipped to AOI	Percent change-GAM	Percent change-VAST
Chinook	222 738 km^2	222 209 km^2	560 335 km^2	−60%	−60%
Chum	352 669 km^2	326 804 km^2	521 916 km^2	−38%	−43%
Pink	513 123 km^2	477 698 km^2	588 819 km^2	−13%	−19%
Sockeye	288 688 km^2	266 188 km^2	582 962 km^2	−50%	−54%

Note: GAM, generalized additive model; VAST, vector autoregressive spatio-temporal; AOI, area of interest.

polygons were compared to those of official EFH shapefiles clipped to the AOI, and the percent difference in EFH area was calculated for each species based on static (Model StaticN) SDMs.

Results

Objective 1: Compare GAM and VAST frameworks for predicting species distributions

Quantitative metrics used for model selection within the respective VAST and GAM frameworks showed agreement across metrics (Table 2). AIC and percent deviance explained favored model structures that accounted for spatial variation in species distributions through time (Models SpatiotA–SpatiotB). Differences across model frameworks emerged in the tests of out-of-sample predictive performance (10-fold cross-validation). 10-fold cross-validation results indicated that VAST models had higher out-of-sample predictive power when compared with parallel GAM structures, as indicated by lower NLL scores (Table 3). Exceptions included the sockeye salmon spatio-temporal models (Models SpatiotA and SpatiotB), where GAMs produced better (lower) negative log-likelihood scores when compared with VAST models, and Model SpatiotB for Chinook salmon, where nonconvergence of the GAMs barred comparison across model frameworks. Diagnostic quantile–quantile plots (Supplementary Figs. S1–S4) indicated that residuals were approximately normally distributed, with slight deviations at the tails for most salmon species, and stronger deviations for Chinook salmon (Supplementary Fig. S1). Maps of residuals (quantile residuals for GAMs, and DHARMa residuals for VAST models) showed greater spatial correlation in GAM residuals compared to VAST residuals, although the degree of correlation appeared to be fairly moderate (Supplementary Figs. S5–S8).

Fig. 2. Side-by-side comparisons of GAM and VAST static model (Model StaticN) predictions for log abundance density (per km^2) in the eastern Bering Sea. Yellow colors denote areas of higher predicted abundance, while darker colors denote areas of lower predicted abundance. Data sources: bathymetry—akgfmaps (Rohan 2023), rivers—USA Rivers and Streams (Esri 2020); Basemap: rnaturalearth (Massicotte and South 2023), Projection: Alaska Albers Conic Equal Area, Datum: NAD83, EPSG code: 3338, Coordinates = Cartesian 2D. GAM, generalized additive model; VAST, vector autoregressive spatio-temporal.

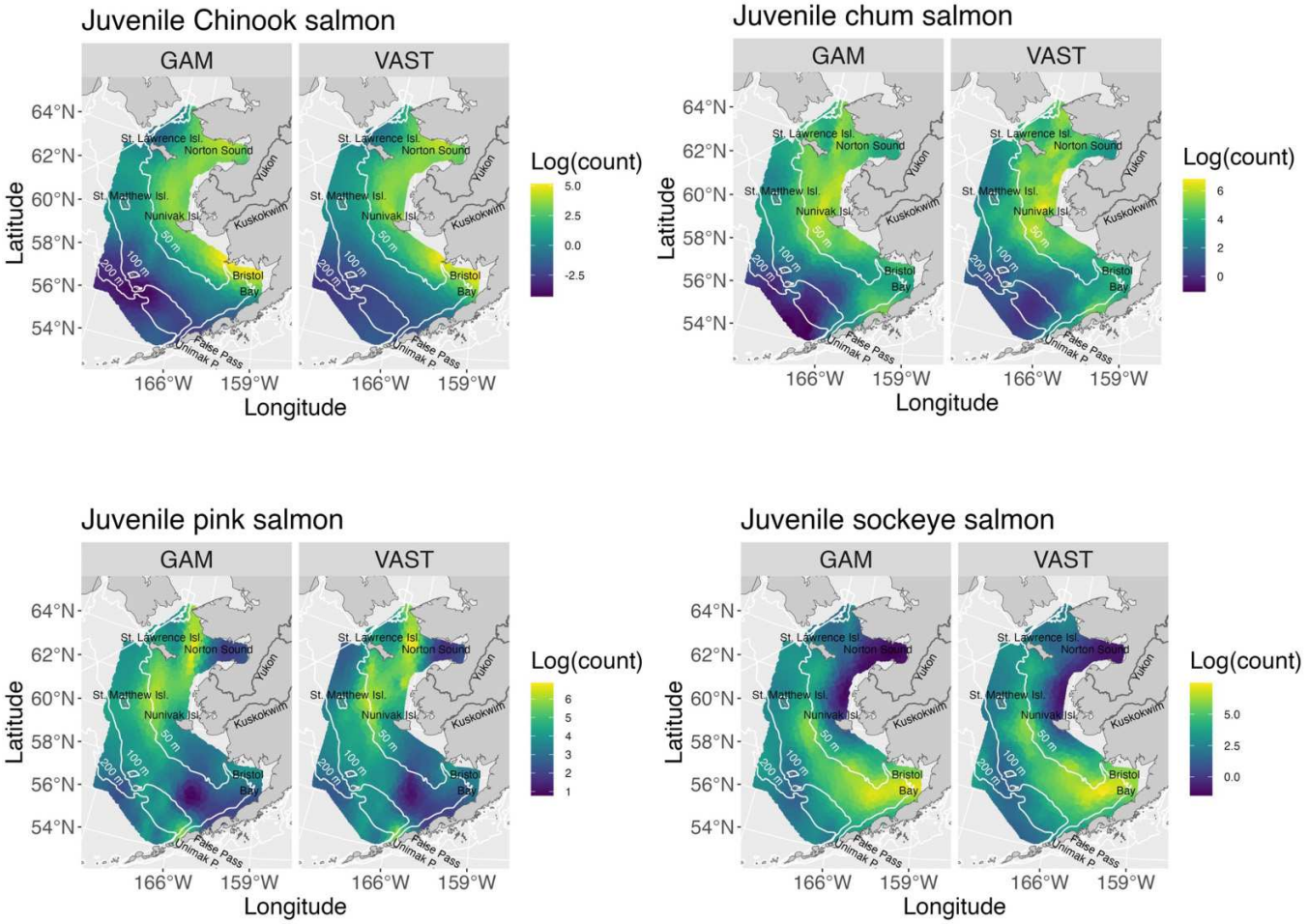

Visual inspection of predicted abundance density across the EBS indicated that GAMs and VAST models predicted largely similar distributions from a qualitative perspective. Species-specific maps of static model (Model StaticN) predictions were nearly identical across the two frameworks (Figs. 2 and 3). However, the VAST framework tended to produce more concentrated static (Model StaticN) distributions of predicted abundance density, leading to model-based EFH (i.e., top 95% of predicted abundance) areas that were 4% (0%–7%) smaller on average than those estimated by the GAMs (Fig. 3; Table 3). Greater differences among the VAST and GAM frameworks were found in maps of spatio-temporal model (Model SpatiotB) predictions (Fig. 4; Supplementary Figs. S10–S12). GAM-predicted Model SpatiotB distributions appeared to deviate more often from patterns predicted by the time-averaged, static model (Model StaticN) and often predicted hotspots of abundance along the margins of the prediction grid. In contrast, VAST-predicted Model SpatiotB distributions appeared to more closely follow the long-term average patterns predicted by static model variants. Maps of model residuals indicated that GAMs tended to under-predict abundance, while VAST models produced both under- and over-predictions across a range of locations and sample years (Supplementary Figs. S5–S8).

Objective 2: Describe juvenile salmon distributions in the EBS

Maps of static model (Model StaticN) predictions of juvenile salmon distributions in the EBS estimated the greatest densities of juvenile salmon within the 50 m isobath of the continental shelf (Figs. 2 and 3). Species-specific differences in predicted distributions were observed for both classes of statistical models. Parallel GAM and VAST model structures predicted similar areas of high abundance for each species, with minor differences among static model predictions (Model StaticN) (Fig. 2) and larger differences among spatio-temporal model predictions (Model SpatiotB) (Fig. 4). The EFH estimates produced using static SDM methods in this study were more spatially concentrated than the current EFH estimates for

Fig. 3. Essential fish habitat maps describing the area representing the top 95% of abundance generated by static generalized additive model (in red) and vector autoregressive spatio-temporal (in blue) model predictions (Model StaticN), with overlapping areas represented in purple. The boundaries of current essential fish habitat definitions are outlined in green, and were sourced from essential fish habitat map shapefiles in Fishery Management Plan for the Salmon Fisheries in the EEZ off Alaska (NPFMC 2024). Data sources: bathymetry—*akgfmaps* (Rohan 2023), rivers—USA Rivers and Streams (Esri 2020); Basemap: *rnaturalearth*, (Massicotte and South 2023), Projection: Alaska Albers Conic Equal Area, Datum: NAD83, EPSG code: 3338, Coordinates = Cartesian 2D.

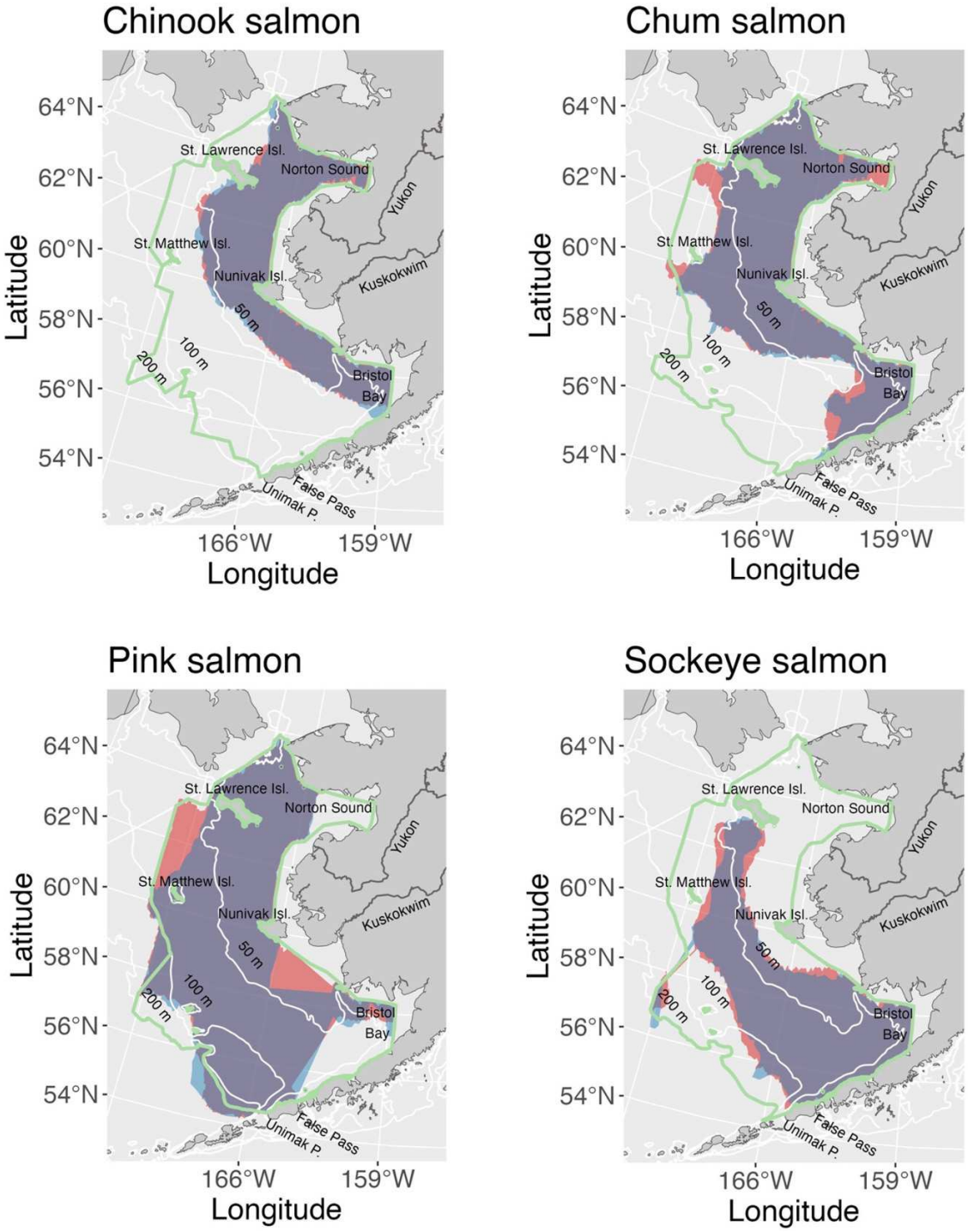

juvenile salmon in the EBS (Table 3), with reductions in EFH area ranging from 13% to 19% (pink salmon) to 60% (Chinook salmon) across VAST and GAM frameworks. All model structures were successfully fit to the data, with the exception of the most flexible spatio-temporal GAM (Model SpatiotB) for juvenile Chinook salmon, which did not converge.

Fig. 4. Maps of GAM (in red) and VAST (in blue) spatio-temporal model predictions (Model SpatiotB) of core essential fish habitat (top 50% of predicted abundance) of juvenile chum salmon in the eastern Bering Sea. The red and blue polygon outlines represent the essential fish habitat areas predicted by GAM and VAST static models (Model StaticN), respectively. Data sources: bathymetry—*akgfmaps* (Rohan 2023), rivers—USA Rivers and Streams (Esri 2020); Basemap: *rnaturalearth* (Massicotte and South 2023), Projection: Alaska Albers Conic Equal Area, Datum: NAD83, EPSG code: 3338, Coordinates = Cartesian 2D. GAM, generalized additive model; vast, vector autoregressive spatio-temporal.

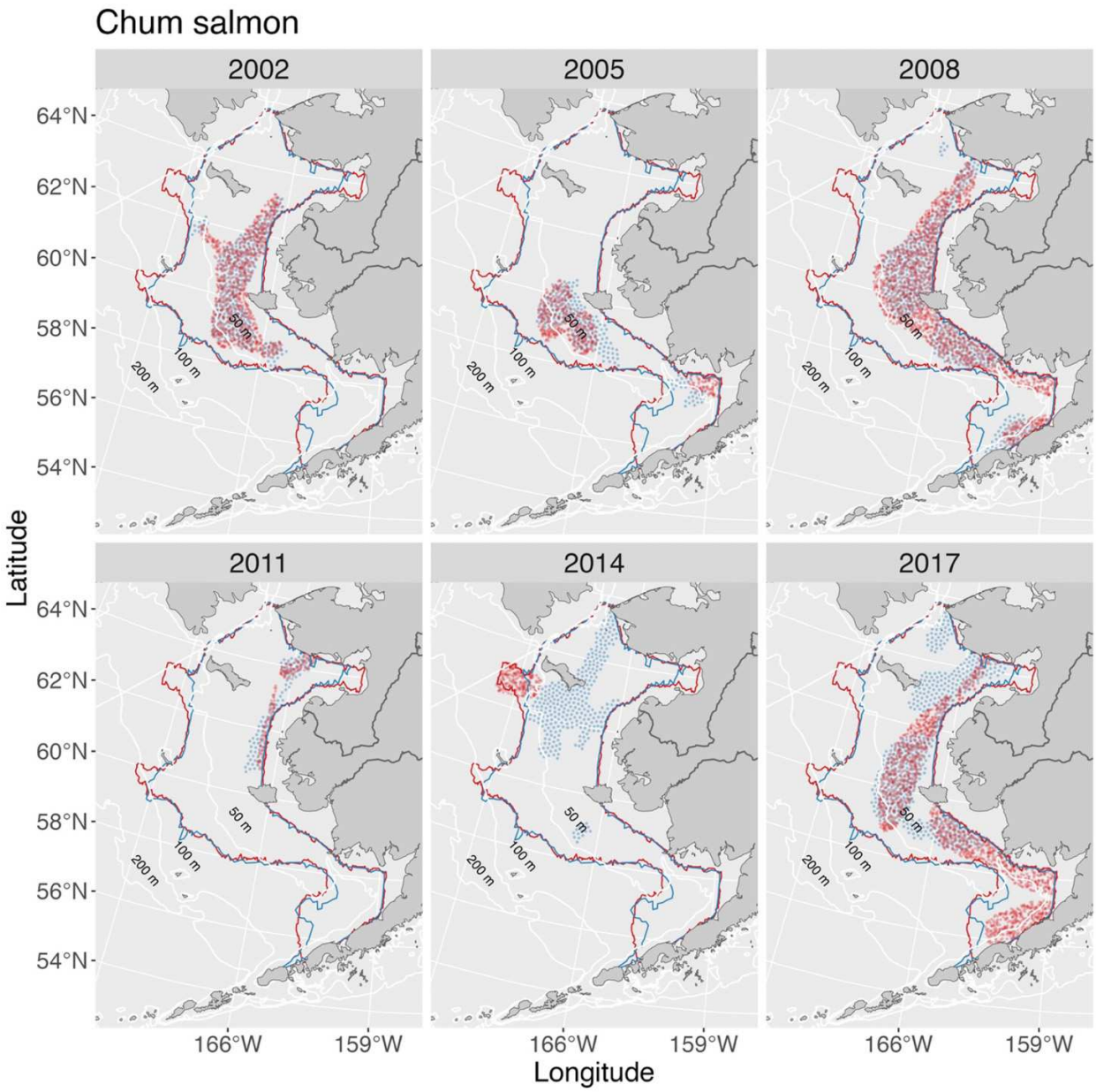

Objective 3: Determine whether juvenile salmon distributions shift through time

To evaluate whether juvenile salmon distributions demonstrate interannual variability, we quantified the strength of evidence for spatial changes in juvenile salmon species distributions through time by comparing the performance of SDMs with either static or dynamic spatial effects. Model selection results indicated greater support for spatio-temporal models that allow juvenile salmon distributions to vary among years for all species (Table 2). The GAM structures with the lowest AIC scores and highest percent deviance explained were the spatio-temporal models with independent spatial fields for each survey year (Model SpatiotB). This was true for all modeled species except juvenile Chinook salmon. The Model SpatiotB GAM failed to fully converge when fit to the Chinook salmon catch data, even after increasing the maximum iteration threshold to 3600. The alternative spatio-temporal GAM structure (Model SpatiotA), representing spatio-temporal autocorrelation, was successfully fit to the Chinook salmon data, produced the lowest AIC score among the Chinook salmon models and explained the

most deviance in the Chinook salmon observations. Model SpatiotA produced the second-lowest AIC scores and second-highest percentages of deviance explained across all other salmon species analyzed in this study.

When out-of-sample predictive performance was compared across the four alternative model structures of varying spatio-temporal complexity, results for both VAST and GAM frameworks showed lower Tweedie deviance scores (NLL, Table 2) for the spatio-temporal model with time-varying distributions (Model SpatiotB) for Chinook, chum, and sockeye, but not pink salmon. These results indicate that for most species, spatio-temporal models that allowed distributions to vary among years better predicted the withheld data (observations) in 10-fold cross-validation. Interestingly, for the species where out-of-sample predictive performance was higher for spatio-temporal models (e.g., Chinook, chum, and sockeye salmon), the constrained spatio-temporal model structure which assumed that species' distribution in a given year were conditional on the distribution in surrounding years (Model SpatiotA) demonstrated higher out-of-sample predictive power.

Visual inspection of model-predicted core (50%) habitat maps from the best-performing spatio-temporal models (Model SpatiotB) provided a more comprehensive picture of distribution changes through time (Fig. 4). While yearly distributions did deviate from the average spatial fields predicted by maps produced by static models (Model StaticN) in terms of size and extent, key habitat areas largely persisted through time in locations predicted by the static spatial models. Furthermore, visual inspection of core essential habitat did not reveal signs of long-term range shifts northward or in any other direction.

Discussion

Our application of static and spatio-temporal SDMs using VAST and GAM frameworks yielded several interesting findings. The GAM and VAST modeling frameworks showed notable differences in performance (Table 2). Statistical metrics (% Deviance Explained, Negative-Log-Likelihood) used to compare the model frameworks indicated that the GAM framework produced models with higher within-sample predictive power (% Deviance Explained), while the VAST framework produced models with higher out-of-sample predictive power (Tweedie negative log-likelihood from cross-validation). This was unexpected based on previous research comparing GAM and VAST model frameworks in SDM applications (Brodie et al. 2020). We also found that GAM spatio-temporal models often predicted hotspots of abundance in ecologically unlikely places, close to the margins of the survey footprint. Reducing the spatial extent of training data and the prediction surface, as well as implementing a first-derivative smoothing penalty, reduced the occurrence of these unlikely abundance hotspots along spatial margins, but it did not completely eliminate them. A simulation analysis exploring differences between Tweedie GAM models in mgcv and Poisson-link delta models (which approximate the Tweedie distribution) in VAST, when confronted with spatially imbalanced input, may help to better identify differences across these two particular estimation platforms.

The predicted EFH spatial footprints from this study encompassing an estimated 95% of the population—pursuant to the current guidelines for Alaska EFH definitions (NPFMC 2024)—were more compact than current official EFH estimates as predicted by the ECDF methods outlined in Echave et al. (2012) (Fig. 3; Table 3). GAMs produced EFH estimates up to 7% larger in extent than those produced by VAST models (Table 3), but would still represent substantial reductions of 13%–60% in EFH area compared to current definitions, across salmon species. Although incorporating environmental covariates into SDM models would facilitate more direct comparisons between SDM- and ECDF-estimated EFH, the results of this study provide initial insights into how they may differ. This is particularly the case in conditions similar to those informing our study, where there exist a limited number of catch rate observations in space and time for a particular life stage of a species, and/or where spatio-temporal data include years with low sampling effort. The ramifications of reducing the spatial extent of EFH in the context of spatial fisheries management are unclear. Refining our understanding of core habitat areas could be helpful for securing stakeholder confidence in future updates to EFH descriptions and in using those habitat areas to prioritize locations for targeted conservation measures, such as gear restrictions and area closures. Shrinking (otherwise changing) the space delineated as "essential" to a species due to changes in quantitative methodologies also requires in-depth conversations among scientists, managers, and the public over management priorities and tradeoffs. This study provides additional information for fisheries researchers to consider when exploring methodologies for quantitatively defining species distributions, hotspots of abundance, and interannual variability in habitat occupation.

The overall better within-sample and out-of-sample predictive performance of the spatio-temporal SDMs (Models SpatiotA–SpatiotB) over the static models (Models StaticN–StaticT) indicates that there is evidence for spatial variation in juvenile salmon distributions in the EBS among years (Table 2). The direction of spatial change in distributions varied according to species, the given year, and the modeling framework, as can be seen in the prediction maps (Fig. 4, Supplementary Figs. S10–S12). Juvenile Chinook, chum, and pink salmon appear to aggregate within or expand across the southern portions of their average distributions in the EBS, even under years spanning the most recent warm climate stanza (2014–2019). There are few proposed hypotheses which touch on the expansion of juvenile salmon distributions in the SEBS. Farley and Trudel (2009) explore the subject, noting that juvenile sockeye salmon were found to have a broader latitudinal distribution during warmer years, when the field of optimal growth rate potential broadened. One substantial challenge of working with migratory species like salmon is capturing intra-annual variation in marine distribution—winter surveys, for example, are particularly difficult to execute in the Bering Sea and remain an area with limited data for salmon. The results of our study suggest that despite interannual variation in juvenile

salmon distributions, the areas of highest abundance-density in each year have largely remained within EFH areas as circumscribed using the top 95% of time-averaged (static) SDM-predicted relative abundance (model StaticT). This might indicate that static EFH definitions provide adequate coverage to meet management objectives. However, the data we used reflected late summer juvenile salmon distributions only, and it is still unclear how future salmon distributions may respond to climate change throughout their marine residence. Much of the present literature on climate-related shifting of fish distributions in the Bering Sea has focused on groundfish species of commercial interest, particularly juvenile walleye pollock (*Theragra chalcogramma*) (Moss et al. 2009; Hollowed et al. 2012; Kotwicki and Lauth 2013; Goodman et al. 2022). Nonetheless, these and other studies of EBS fisheries oceanography and trophic ecology have developed a foundation of EBS ecological theory from which to guide future research into interannual variability in Pacific salmon distributions.

Similar to prior studies that have applied SDM frameworks to define EFH (Laman et al. 2018; Harris et al. 2023), our results indicate that an SDM approach can effectively refine EFH definitions where data are limited and existing EFH definitions are broad. Further study of the similarities and differences among GAM and VAST frameworks when utilized for marine habitat delineation would be beneficial for informing managers of the tradeoffs when selecting one or more SDM frameworks to guide policy decisions. The most recent updates to EFH descriptions in Alaska were developed through an SDM ensemble (e-SDM) approach, which leveraged maximum entropy models, presence–absence GAMs, hurdle GAMs, and two forms of standard GAMs, to reduce bias and produce better uncertainty estimates (Harris et al. 2023; Pirtle et al. 2024). The e-SDM approach to spatial fisheries management has seen expanded use in other regions of the world as well, including the Mediterranean (Quinci et al. 2022; Panzeri et al. 2024), and the China Seas (Liu et al. 2023; Sun et al. 2024). In summary, the integration of diverse SDM frameworks such as GAMs and VAST models in ensemble approaches demonstrates significant potential for refining EFH descriptions and enhancing spatial fisheries management strategies. Continued exploration and comparison of these methods may help to inform policy decisions in the face of environmental variability and change.

Acknowledgements

We are grateful for the efforts of the many technicians and biologists who gathered and processed the Bering–Arctic–Subarctic Integrated Survey data used in this manuscript. Lisa Eisner, Ed Farley, Wes Strasburger, and Jordan Watson provided constructive feedback on project development and early analyses. We thank Lukas DeFilippo and Katherine Miller for helpful comments on an earlier draft. We also thank the three anonymous peer reviewers who helped usher this manuscript to publication. This project was funded in part by the Habitat Conservation Division, Alaska Regional Office, National Marine Fisheries Service. The scientific results and conclusions, as well as any views or opinions expressed herein, are those of the author(s) and do not necessarily reflect those of NOAA or the Department of Commerce.

Article information

History dates

Received: 10 May 2024
Accepted: 22 January 2025
Accepted manuscript online: 7 April 2025
Version of record online: 8 May 2025

Copyright

Data availability

Data generated or analyzed during this study are available in the following repositories: Github, DOI: https://doi.org/10.5281/zenodo.14812743; Alaska Ocean Observing System Ocean Data Explorer, portal.aoos.org.

Author information

Author ORCIDs

Lilian K.G. Hart https://orcid.org/0009-0001-4097-1480
James T. Thorson https://orcid.org/0000-0001-7415-1010

Author contributions

Conceptualization: LKGH, CJC, EMY
Data curation: JAD
Formal analysis: LKGH
Funding acquisition: LKGH, CJC, EMY, JLP
Investigation: LKGH
Methodology: LKGH, CJC, FJM, JTT
Project administration: CJC
Resources: CJC, EMY, FJM, JTT, JLP
Software: LKGH, JTT
Supervision: CJC, EMY, FJM
Visualization: LKGH
Writing – original draft: LKGH
Writing – review & editing: CJC, EMY, FJM, JTT, JLP

Competing interests

The authors declare there are no competing interests.

Funding information

This research was supported by the National Marine Fisheries Service, Office of Habitat Conservation, Essential Fish Habitat Innovation and Advancement Funding Program; the North Pacific Research Board (Graduate Student Research Award); the NOAA Quantitative Ecology and Socioeconomics Training Program at the University of Alaska Fairbanks; the University of Alaska Fairbanks (Graduate School Degree Completion Fellowship); and the Ken Turner Memorial Fellowship.

Supplementary material

Supplementary data are available with the article at https://doi.org/10.1139/cjfas-2024-0137.

References

Barnes, C.L., Essington, T.E., Pirtle, J.L., Rooper, C.N., Laman, E.A., Holsman, K.K., et al. 2022. Climate-informed models benefit hindcasting but present challenges when forecasting species–habitat associations. Ecography, **2022**. doi:10.1111/ecog.06189. PMID: 34987352.

Beamish, R.J. 2018. The ocean ecology of Pacific salmon and trout. American Fisheries Society. doi:10.47886/9781934874455.ch5.

Bivand, R., Keitt, T., and Rowlingson, B. 2023. rgdal: bindings for the 'Geospatial' data abstraction library. R package version 1.6-5. Available from https://CRAN.R-project.org/package=rgdal.

Bivand, R.S., Pebesma, E.J., and Gomez-Rubio, V. 2013. Applied spatial data analysis with R. 2nd ed. Springer, NY. Available from https://asdar-book.org/. doi:10.1007/978-1-4614-7618-4.

Brodie, S., Abrahms, B., Bograd, S.J., Carroll, G., Hazen, E.L., Muhling, B.A., et al. 2021. Exploring timescales of predictability in species distributions. Ecography, **44**. doi:10.1111/ecog.05504.

Brodie, S.J., Thorson, J.T., Carroll, G., Hazen, E.L., Bograd, S., Haltuch, M.A., et al. 2020. Trade-offs in covariate selection for species distribution models: a methodological comparison. Ecography, **43**(1): 11–24. doi:10.1111/ecog.04707.

Burnham, K.P., and Anderson, D.R. 2002. Model selection and multimodel inference: a practical information-theoretic approach. 2nd ed. Springer, New York.

Charsley, A.R., Grüss, A., Thorson, J.T., Rudd, M.B., Crow, S.K., David, B., et al. 2023. Catchment-scale stream network spatio-temporal models, applied to the freshwater stages of a diadromous fish species, longfin eel (*Anguilla dieffenbachii*). Fish. Res. **259**(106583): 106583. doi:10.1016/j.fishres.2022.106583.

Dunn, P.K., and Smyth, G.K. 1996. Randomized quantile residuals. J. Comput. Graphical Stat. **5**: 236–244. doi:10.1080/10618600.1996.10474708.

Echave, K., Eagleton, M., Farley, E.V., Jr., and Orsi, J.A. 2012. A refined description of essential fish habitat for Pacific salmon within the US exclusive economic zone in Alaska (NMFS-AFSC-236). National Marine Fisheries Service.

Environment Protection and Biodiversity Conservation Act, C2024C00598. 1999. Available from https://www.legislation.gov.au/C2004A00485/latest/text.

Esri. 2020. USA Rivers and Streams. [Feature Layer]. Esri, National Atlas of the United States, United States Geological Survey. Available from https://www.arcgis.com/home/item.html?id=8206e517c2264bb39b4a0780462d5be1.

EU Action Plan: Protecting and Restoring Marine Ecosystems for Sustainable and Resilient Fisheries (COM(2023)103). 2023. European Union. Available from https://oceans-and-fisheries.ec.europa.eu/document/download/728a02d1-1983-4f92-bd8a-cce23f270c98_en?filename=COM-2023-102_en.pdf.

FAO. Code of Conduct for Responsible Fisheries. 1995. Available from https://www.fao.org/4/v9878e/v9878e00.htm [accessed 26 September 2024].

Farley, E.V., and Trudel, M. 2009. Growth rate potential of juvenile sockeye salmon in warmer and cooler years on the eastern Bering Sea shelf. J. Mar. Biol. **2009**. doi:10.1155/2009/640215.

Farley, E.V., Murphy, J.M., Cieciel, K., Yasumiishi, E.M., Dunmall, K., Sformo, T., and Rand, P. 2020. Response of Pink salmon to climate warming in the northern Bering Sea. Deep Sea Res. Part II, **177**: 104830. doi:10.1016/j.dsr2.2020.104830.

Farley, E.V., Murphy, J.M., Wing, B.W., Moss, J.H., and Middleton, A. 2005. Distribution, migration pathways, and size of western Alaska juvenile salmon along the eastern Bering Sea shelf. Alaska Fish. Res. Bull. **11**(1): 15–26.

Gombin, J., Vaidyanathan, R., and Agafonkin, V. 2020. Concaveman: a very fast 2D concave hull algorithm. R package version 1.1.0. Available from https://CRAN.R-project.org/package=concaveman. doi:10.32614/CRAN.package.concaveman.

Goodman, M.C., Carroll, G., Brodie, S., Grüss, A., Thorson, J.T., Kotwicki, S., et al. 2022. Shifting fish distributions impact predation intensity in a sub-arctic ecosystem. Ecography, **2022**(9). doi:10.1111/ecog.06084. PMID: 34987352.

Grüss, A., Thorson, J.T., Anderson, O.F., O'Driscoll, R.L., Heller-Shipley, M., and Goodman, S. 2023. Spatially varying catchability for integrating research survey data with other data sources: case studies involving observer samples, industry-cooperative surveys, and predators as samplers. Can. J. Fish. Aquat. Sci.doi:10.1139/cjfas-2023-0051. PMID: 37942173.

Grüss, A., Walter, J.F., Babcock, E.A., Forrestal, F.C., Thorson, J.T., Lauretta, M.V., and Schirripa, M.J. 2019. Evaluation of the impacts of different treatments of spatio-temporal variation in catch-per-unit-effort standardization models. Fish. Res. **213**: 75–93. doi:10.1016/j.fishres.2019.01.008.

Harris, J., Laman, E.A., Pirtle, J.L., Siple, M.C., Rooper, C.N., Hurst, T.P., and Conrath, C.L. 2022. Advancing model-based essential fish habitat descriptions for north Pacific species in the Aleutian Islands. U.S. Department of Commerce, NOAA Technical Memorandum NMFS-AFSC-458. 406p. Available from https://repository.library.noaa.gov/view/noaa/48658. doi:10.25923/y5gc-nk42.

Harris, J., Pirtle, J.L., Laman, E.A., Siple, M.C., and Thorson, J.T. 2023. An ensemble approach to species distribution modelling reconciles systematic differences in estimates of habitat utilization and range area. J. Appl. Ecol. **61**: 351–364. doi:10.1111/1365-2664.14559.

Hollowed, A.B., Barbeaux, S.J., Cokelet, E.D., Farley, E., Kotwicki, S., Ressler, P.H., et al. 2012. Effects of climate variations on pelagic ocean habitats and their role in structuring forage fish distributions in the Bering Sea. Deep Sea Res. Part II, **65–70**: 230–250. doi:10.1016/j.dsr2.2012.02.008.

Kotwicki, S., and Lauth, R.R. 2013. Detecting temporal trends and environmentally-driven changes in the spatial distribution of bottom fishes and crabs on the eastern Bering Sea shelf. Deep Sea Res. Part II, **94**: 231–243. doi:10.1016/j.dsr2.2013.03.017.

Laman, E.A., Pirtle, J.L., Harris, J., Siple, M.C., Rooper, C.N., Hurst, T.P., and Conrath, C.L. 2022. Advancing model-based essential fish habitat descriptions for north Pacific species in the Bering Sea. U.S. Department of Commerce, NOAA Technical Memorandum NMFS-AFSC-459. 538p. Available from https://repository.library.noaa.gov/view/noaa/48659. doi:10.25923/y5gc-nk42.

Laman, E.A., Rooper, C.N., Turner, K., Rooney, S., Cooper, D.W., and Zimmermann, M. 2018. Using species distribution models to describe essential fish habitat in Alaska. Can. J. Fish. Aquat. Sci. **75**(8): 1230–1255. doi:10.1139/cjfas-2017-0181.

Langan, J.A., Cunningham, C.J., Watson, J.T., and McKinnell, S. 2024. Opening the black box: new insights into the role of temperature in the marine distributions of Pacific salmon. Fish Fish. **25**(4): 551–568. doi:10.1111/faf.12825.

Liu, S., Tian, Y., Liu, Y., Alabia, I.D., Cheng, J., and Ito, S.I. 2023. Development of a prey-predator species distribution model for a large piscivorous fish: a case study for Japanese Spanish mackerel *Scomberomorus niphonius* and Japanese anchovy *Engraulis japonicus*. Deep Sea Res. Part II, **207**(105227): 105227. doi:10.1016/j.dsr2.2022.105227.

Malta MedFish4Ever Ministerial Declaration. 2017. Ministerial Conference on the Sustainability of Mediterranean Fisheries. Available from https://gfcmsitestorage.blob.core.windows.net/website/3.MedFish4Ever/declaration/2017-03-30-declaration-malta.pdf.

Massicotte, P., and South, A. 2023. Rnaturalearth: world map data from natural earth. R package version 0.3.2. Available from https://CRAN.R-project.org/package=rnaturalearth. doi:10.32614/CRAN.package.rnaturalearth.

Maunder, M.N., Thorson, J.T., Xu, H., Oliveros-Ramos, R., Hoyle, S.D., Tremblay-Boyer, L., et al. 2020. The need for spatio-temporal modeling to determine catch-per-unit effort based indices of abundance and associated composition data for inclusion in stock assessment models. Fish. Res. **229**: 105594. doi:10.1016/j.fishres.2020.105594.

McKelvey, D., and Williams, K. 2018. Abundance and distribution of age-0 walleye Pollock in the eastern Bering Sea shelf during the Bering Arctic Subarctic Integrated Survey (BASIS) in 2014 (NMFS-AFSC-382). National Marine Fisheries Service. Available from https://repository.library.noaa.gov/view/noaa/18698.

Moss, J.H., Farley, E.V., Feldmann, A.M., and Ianelli, J.N. 2009. Spatial distribution, energetic status, and food habits of eastern Bering Sea age-

0 walleye pollock. Trans. Am. Fish. Soc. **138**(3): 497–505. doi:10.1577/T08-126.1.

Mueter, F.J., and Litzow, M.A. 2008. Sea ice retreat alters the biogeography of the Bering Sea continental shelf. Ecol. Appl. **18**(2): 309–320. doi:10.1890/07-0564.1. PMID: 18488598.

Murphy, J., Garcia, S., Dimond, J., Moss, J., Sewall, F., Strasburger, W., et al. 2021. Northern Bering Sea surface trawl and ecosystem survey report, 2019 (NMFS-AFSC-423). Alaska Fisheries Science Center.

Murphy, J.M., Howard, K.G., Gann, J.C., Cieciel, K.C., Templin, W.D., and Guthrie, C.M. 2017. Juvenile Chinook salmon abundance in the northern Bering Sea: implications for future returns and fisheries in the Yukon River. Deep Sea Res. Part II, **135**: 156–167. doi:10.1016/j.dsr2.2016.06.002.

North Pacific Fishery Management Council (NPFMC). 2024. Fishery Management Plan for the Salmon Fisheries in the EEZ off Alaska. 1007 West Third Avenue, #400 Anchorage, AK 99501. Available from https://www.npfmc.org/wp-content/PDFdocuments/fmp/Salmon/SalmonFMP.pdf, https://www.npfmc.org/wp-content/PDFdocuments/fmp/Salmon/SalmonFMPAppendix.pdf.

Panzeri, D., Russo, T., Arneri, E., Carlucci, R., Cossarini, G., Isajlović, I., et al. 2024. Identifying priority areas for spatial management of mixed fisheries using ensemble of multi-species distribution models. Fish Fish. **25**(2): 187–204. doi:10.1111/faf.12802.

Pebesma, E. 2018. Simple features for R: standardized support for spatial vector data. R J. **10**(1): 439–446. doi:10.32614/RJ-2018-009.

Pebesma, E.J., and Bivand, R.S. 2005. Classes and methods for spatial data in R. R News, **5**(2). Available from https://cran.r-project.org/doc/Rnews/. doi:10.32614/CRAN.package.sp.

Pirtle, J.L, Laman, E.A., Harris, J., Siple, M.C., Rooper, C.N., Hurst, T.P., et al. 2023. Advancing model-based essential fish habitat descriptions for north Pacific species in the Gulf of Alaska. U.S. Department of Commerce, NOAA Technical Memorandum NMFS-AFSC-468. 541p. Available from https://repository.library.noaa.gov/view/noaa/49987. doi:10.25923/ygdf-5f65.

Pirtle, J.L., Laman, E.A., Harris, J., Siple, M.C., Rooper, C.N., Hurst, T.P., et al. 2024. Synthesis report: advancing model-based essential fish habitat descriptions and maps for north Pacific species. U.S. Department of Commerce, NOAA Technical Memo. NMFS-F/AKR-28. 295p. doi:10.25923/jvpx-ck45.

Quinci, E.M., Torri, M., Cuttitta, A., and Patti, B. 2022. Predicting potential spawning habitat by ensemble species distribution models: the case study of European anchovy (*Engraulis encrasicolus*) in the Strait of Sicily. Water, **14**(9): 1400. doi:10.3390/w14091400.

Rohan, S. 2023. akgfmaps: Alaska Groundfish and Ecosystem Survey Area Mapping. R package version 3.3.0.

Shelton, A.O., Sullaway, G.H., Ward, E.J., Feist, B.E., Somers, K.A., Tuttle, V.J., et al. 2021. Redistribution of salmon populations in the northeast Pacific Ocean in response to climate. Fish Fish. **22**(3): 503–517. doi:10.1111/faf.12530.

Shono, H. 2008. Application of the Tweedie distribution to zero-catch data in CPUE analysis. Fish. Res. **93**(1): 154–162. doi:10.1016/j.fishres.2008.03.006.

Sun, Y., Zhang, H., Jiang, K., Xiang, D., Shi, Y., Huang, S., et al. 2024. Simulating the changes of the habitats suitability of chub mackerel (*Scomber japonicus*) in the high seas of the North Pacific Ocean using ensemble models under medium to long-term future climate scenarios. Mar. Pollut. Bull. **207**(116873): 116873. doi:10.1016/j.marpolbul.2024.116873. PMID: 39180964.

Thorson, J.T. 2019a. Forecast skill for predicting distribution shifts: a retrospective experiment for marine fishes in the eastern Bering Sea. Fish Fish. **20**(1): 159–173. doi:10.1111/faf.12330.

Thorson, J.T. 2019b. Guidance for decisions using the vector autoregressive spatio-temporal (VAST) package in stock, ecosystem, habitat and climate assessments. Fish. Res. **210**: 143–161. doi:10.1016/j.fishres.2018.10.013.

Thorson, J.T., and Barnett, L.A.K. 2017. Comparing estimates of abundance trends and distribution shifts using single- and multispecies models of fishes and biogenic habitat. ICES J. Mar. Sci. **74**(5): 1311–1321. doi:10.1093/icesjms/fsw193.

Thorson, J.T., Barnes, C.L., Friedman, S.T., Morano, J.L., and Siple, M.C. 2023. Spatially varying coefficients can improve parsimony and descriptive power for species distribution models. Ecography, **2023**(5): e06510. doi:10.1111/ecog.06510.

Thorson, J.T., Cunningham, C.J., Jorgensen, E., Havron, A., Hulson, P.-J.F., Monnahan, C.C., and von Szalay, P. 2021. The surprising sensitivity of index scale to delta-model assumptions: recommendations for model-based index standardization. Fisheries Research, **233**, 105745. doi:10.1016/j.fishres.2020.105745.

Wickham, H. 2016. ggplot2: elegant graphics for data analysis. Springer-Verlag, New York. Available from https://ggplot2.tidyverse.org.

Wood, S.N. 2006. Introducing GAMs. *In* Generalized additive models. CRC Press. pp. 121–140. doi:10.1201/9781420010404.

Wood, S.N., Pya, N., and Saefken, B. 2016. Smoothing parameter and model selection for general smooth models. J. Am. Stat. Assoc. **111**: 1548–1575. doi:10.1080/01621459.2016.1180986.

Yasumiishi, E.M., Cieciel, K., Andrews, A.G., Murphy, J., and Dimond, J.A. 2020. Climate-related changes in the biomass and distribution of small pelagic fishes in the eastern Bering Sea during late summer, 2002–2018. Deep Sea Res. Part II, **181–182**: 104907. doi:10.1016/j.dsr2.2020.104907.